Design and Characterization of High-Power Optically Pumped Green-Emitting Semiconductor Disk Lasers Using Second-Harmonic Generation

Alexander Hein and Susanne Menzel

Frequency-doubled optically pumped VECSELs which are aimed for an emission wavelength of 520 nm are presented. Layer design as well as experimental results are discussed. Differential quantum and slope efficiencies in the fundamental regime as high as 75 % and 57 %, respectively, are demonstrated. An optical output power for the second harmonic of more than 7 W is achieved.

1. Introduction

Although green semiconductor lasers have been realized in the gallium nitride material system [1], the available output powers of these are rather small. On the other hand, semiconductor disk lasers also called Vertical-External-Cavity Surface-Emitting Lasers (VECSELs) with fundamental emission in the range of 1000–1100 nm can provide high output powers of several watts in the green spectral range [2, 3] when combined with intra-cavity second-harmonic generation. Even though the VECSEL may be considered a relatively large and bulky source in the semiconductor laser family, rather compact cavities with efficient green output slightly below the watt level were already demonstrated [4, 5].

2. Layer Design

Major elements in the layer design of the presented VECSELs are a dielectric anti-reflection (AR) coating, a Resonant Periodic Gain (RPG) structure, and a binary rear Distributed Bragg Reflector (DBR). Contrary to our previous work [6], we disclaimed to follow the double-band DBR approach since, for the target wavelength of 1040 nm, the overall layer thickness of such a structure could be well beyond 7 µm, thus, making defect-free growth more difficult. For the DBR, an alternating AlGaAs/AlAs stack of 56 layers in total was chosen, aimed for high reflectivity at 1040 nm. The RPG structure is composed of periodically arranged InGaAs quantum wells (QWs) with a thickness of 7 nm which are embedded into GaAs. Strain compensation of the QWs was realized by using two different compositions of GaAsP in the pump light absorbing barriers. The AR coating is a TiO_2 layer applied by ion-beam sputter deposition. The surface reflectivities of the pump and the emission wavelength are calculated as 4 % and 10 % for incident angles of 25 ° and 0 °, respectively. In order to tune the micro-cavity resonance, an AlGaAs confinement layer is placed between the gain structure and the dielectric coating.

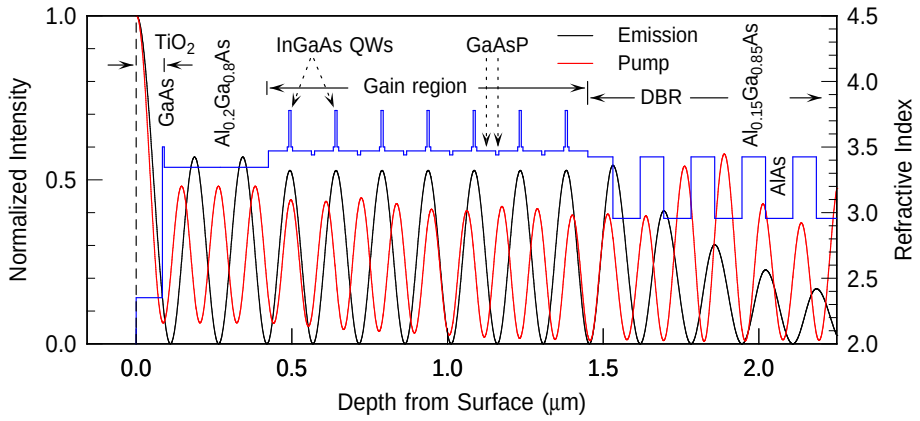

Fig. 1: Structure layout, indicated by the refractive index, and field intensities of the emission and the pump wavelength.

The structure layout is depicted in Fig. 1. Although the Bragg reflector mainly provides a high reflectivity for the emission wavelength, the structure enables a second resonance since the gold metalization at the end of the DBR acts as a reflector for the pump light.

3. Characterization

3.1 Structure quality

In a fast preliminary characterization by utilizing locally resolved photoluminescence (PL), the internal quality of the fabricated laser structures can be visualized. The samples are excited with the pump laser which is defocussed and illuminates the whole chip area as depicted in the center part of Fig. 2. Any structural defects arising from strain or processing errors are typically seen as dark lines in a cross-hatch pattern or simply appear as dark spots. According to the surface photograph (left) and the PL image (center) the laser structure shows no greater structural impairs. However, there are soldering imperfections and residues of the etch-stop layers. After extensive operation (right), these defects appear to have been intensified. This defect "growth" is attributed to "burn-ins" of the previously small defects/residues at high optical input of the pump. Any major detrimental impairs were not observed so far.

Fig. 2: Surface picture of a sample where substrate residues and solder imperfections are visible (left). Locally resolved photoluminescence images of a sample before (center) and after (right) laser operation. The sample was illuminated with the pump laser diode emitting at 804 nm.

3.2 Spectral characteristics

For further characterization of our structures, reflectivity and photoluminescence (PL) spectra are recorded as shown in Fig. 3. The Bragg reflector is centered around 1035 nm where highest reflectivity is provided. At the pump wavelength of around 804 nm, the reflectivity is strongly suppressed due to the AR coating. The excitonic absorption dip is located within the stop band around 1010–1020 nm. The PL peak from the QWs which is almost congruent with the excitonic absorption dip was designed to be around 1020 nm at room temperature corresponding to a detuning of 20 nm with respect to the micro-cavity resonance. The micro-cavity resonance is determined from PL spectra indicated in the right part of Fig. 3, where the temperature is varied between 0 °–90 °C. From the distinct peak evolving around 1049–1057 nm, the optical resonance is estimated to be around 1055 nm when accounted for a resonable temperature rise during operation. The red-shift happens at a rate of 0.09 nm/K. The determined value results in a 15 nm upward offset

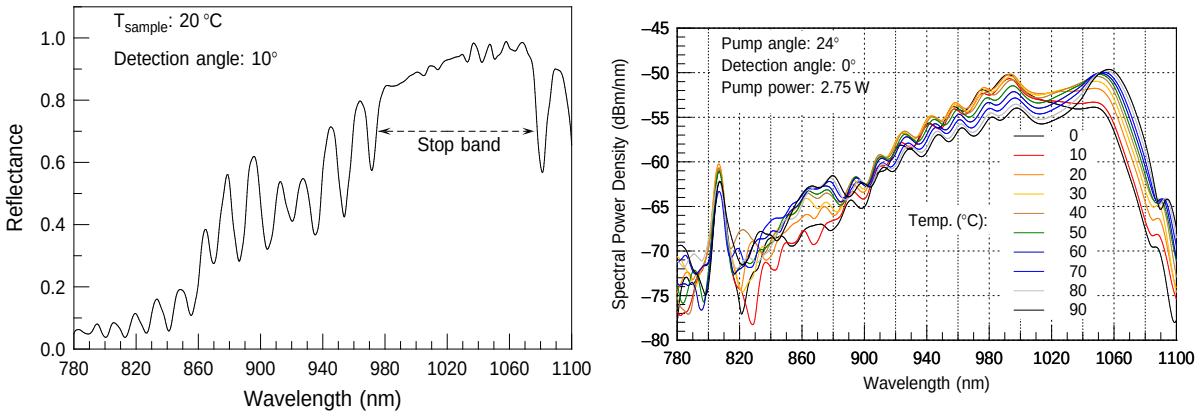

Fig. 3: Reflectivity spectrum (left) and the corresponding photoluminescence (right). The resonance at normal incidence is determined from the evolving peak in the optical spectra of the PL measurements. The pump radiation is visible as a distinct peak at around 804 nm.

to the target of 1040 nm. Reasons herefore are flux deviations during the growth process, insufficient incorporation of phophorous in the barrier layers, and thickness deviations of the AR coating. This detuning of approximately 35–40 nm can be considered large but would allow laser operation at elevated temperatures.

4. Fundamental Output

To effectively remove the heat from the devices during operation, these were soldered onto 300 µm thick diamond heatspreaders which in turn were soldered to either copper heatsinks or water cooled microchannel mounts. The output and absorptance characteristics of a microchannel mounted device are presented in Fig. 4 for various sizes of the pump spot. The microchannel mounts were not temperature controlled or stabilized. The cooling water temperature was set to 6 °C, while the ambient temperature was 20 °C. As the external mirror for the cavity an output coupler with a radius of curvature of 150 mm and a specified reflectivity of 98 % at a wavelength of 1035 nm was used. The pump radiation

was incident at an angle of 24° to normal. In case of the microchannel mount, a maximum output power of 14.1 W was achieved in the free running mode. The degree of absorptance for the pump ranged from 95–96 %. The spectral emission of the devices is rather broad, especially at high excitation. The peak wavelength shift over the absorbed optical power range was approximately 20 nm starting at around 1041 nm at threshold and increased to 1060 nm at the highest excitation. Due to the gradient on our wafers, the large pump spot, and the temperature gradient within, the spectral emission is broadend. Structures

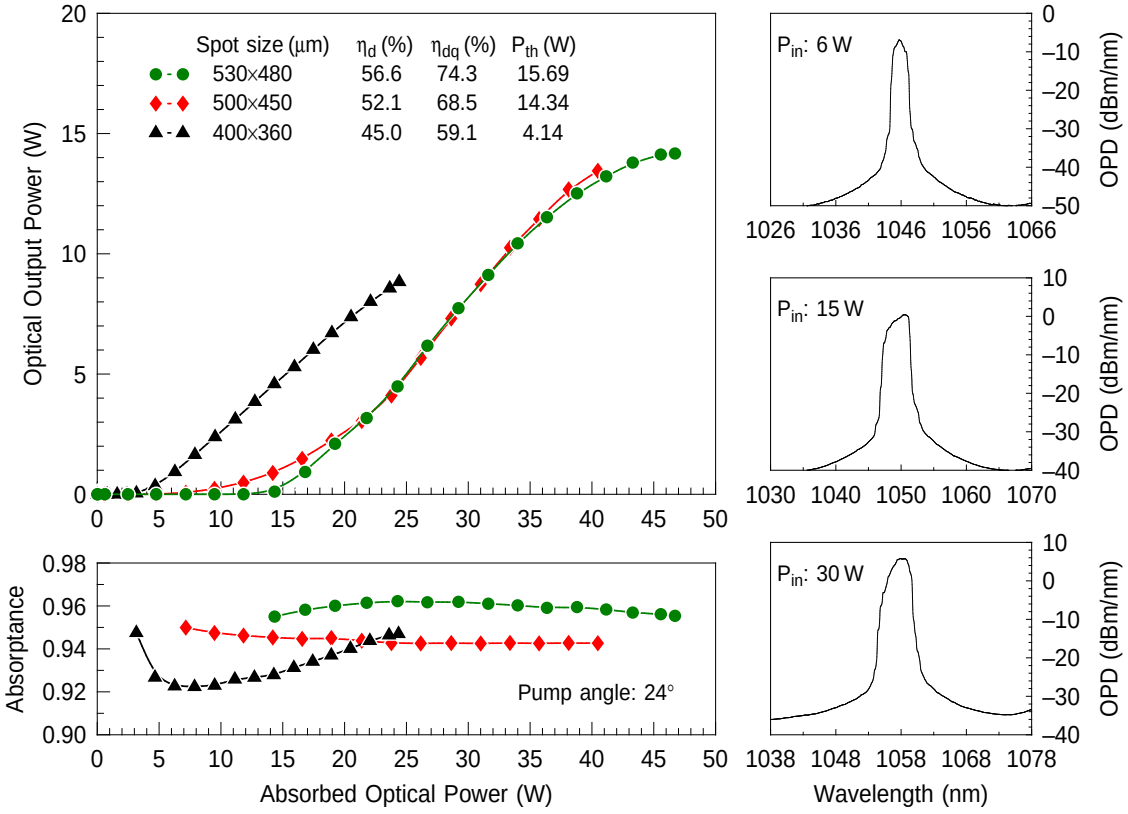

Fig. 4: Left: fundamental output and absorptance characteristics for different pump spot sizes. Slope η_d, differential quantum efficiency η_{dq}, and threshold power are calcultaed from fits. The measurements were performed with an outcoupling reflectivity of 98 % at 1035 nm. Right: optical spectra at different pump excitation levels with the increasing spectral width and red-shift.

that were soldered to copper heatsinks were temperature controlled and stabilized with a thermoelectric peltier cooler. The heatsink temperature was set to 16 °C in all presented measurements. Lower temperatures could not be sustained by the capacity of the cooling system during high power laser operation. The device was operated with two different outcoupling reflectivities, namely 98 % and 97 %. Because of thickness variations of the applied AR coating, the device was pumped at a slightly smaller angle of 20° where the surface reflectivity for the pump was smallest. The characteristics are given in Fig. 5. The maximum achieved output power was 18 W and 12.7 W, respectively. However, the pump spot was smaller when the device was operated with the lower outcoupling reflectivity. The absorptance was nearly identical to the previous device ranging between 94–96 %. For the higher outcoupling reflectivity and the larger pump spot we observed what may

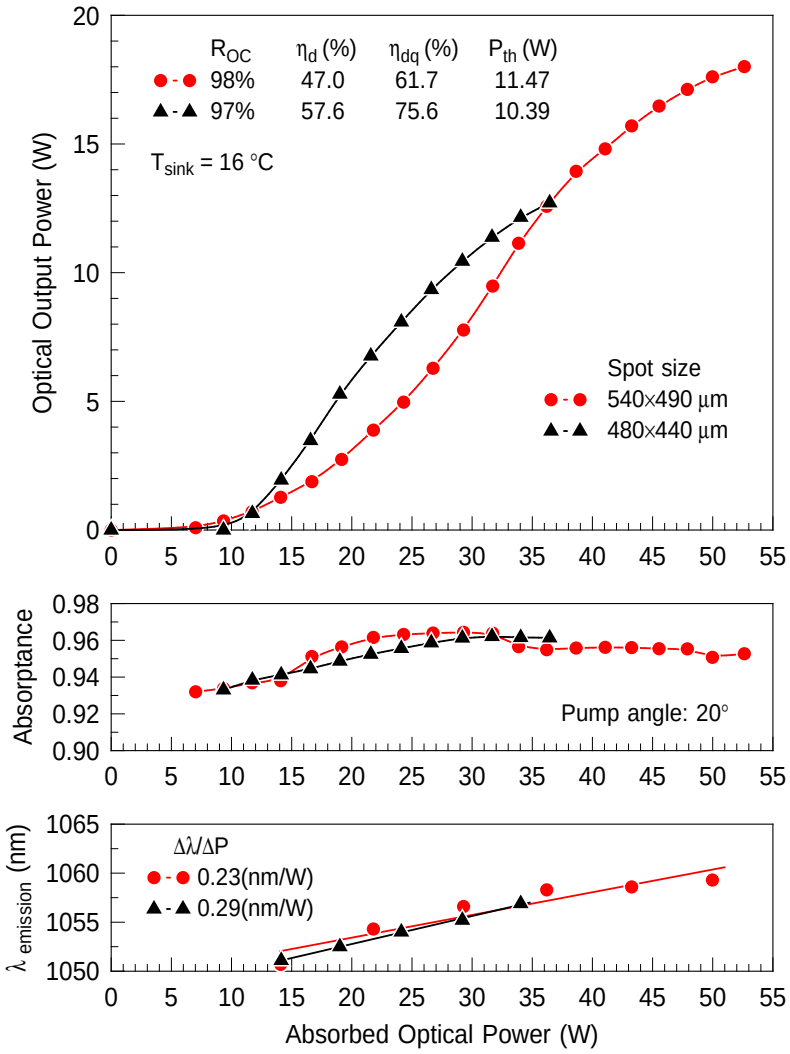

Fig. 5: Fundamental output of a temperature-controlled device. Absorptance and the spectral shift of the peak wavelength are shown in the lower parts of the figure. The spectral shift is indicated as a rate per unit of absorbed pump power and is determined from a linear fit.

be called "nonlinear behaviour" of the optical ouput. It seems that due to the larger than intended detuning between peak gain and micro-cavity resonance, the slope above threshold gradually increases until an optimum condition is reached around 25 W of absorbed power where the overlap of gain and micro-cavity resonance is best. The slope remains constant until approximately 37 W. Beyond that point thermal rollover gradually starts to set in. Accounting for this particular interval of the output curve, a slope efficiency higher than 65 % is achieved and would correspond to a differential quantum efficiency of more than 85 %. A higher efficiency in VECSELs was only achieved in an in-well pumped structure [7] where a tunable titanium-sapphire laser was used as the pump source. When considering an average slope of the output curve, the efficiency drops to 47 % with a corresponding differential quantum efficiency of 61 %. For the smaller spot size and higher outcoupling transmittance, the slope and differential quantum efficiency are above 57 % and 75 %, respectively, in the linear regime. The rate of the spectral shift per unit of

dissipated heat is with 0.44 nm/W and 0.60 nm/W, respectively, indicating better heat dissipation for the bigger spot size. However, better values as low as 0.1 nm/W can be obtained [8], but this rate also strongly depends on the detuning.

5. Second-Harmonic Output

The general cavity configuration for frequency doubling is illustrated in Fig. 6 and is similar to the one in our privious work [6]. Polarization and wavelength were controlled via a 4 mm thick birefringent quartz filter (BRF) located in the longer cavity arm. The BRF was set at the Brewster angle in order to suppress the σ-polarization (TE). The folding angle of the cavity was set to 30 ° corresponding to 15 ° of incidence with respect to beam propagation. The nonlinear crystals were placed in close proximity of the plane mirror due to the location of the second beam waist where the intensity is highest and the conversion most efficient. The nonlinear crystals were not temperature controlled or stabilized. The output was generated in a compact, folded, V-shaped cavity with foot prints of 89 mm for the longer and 32–33 mm for the shorter arm, depending on the crystal length and crystal material. The crystal facest are AR coated for the fundamental and the second harmonic in order to suppress etalon effects. The heat sink temperature was kept at 0 °C facilitating

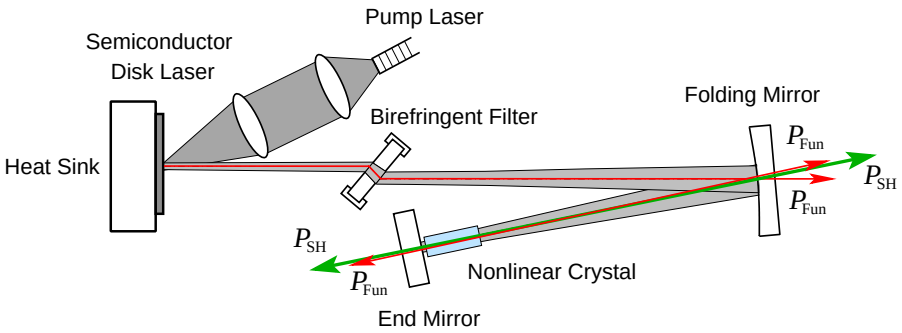

Fig. 6: Folded cavity with wavelength and polarization control via the BRF, and the nonlinear crystal for second-harmonic generation.

emission at a wavelength explicitly shorter than the favored micro resonance. Output characteristics of the second-harmonic regime are shown in Fig. 7 for different nonlinear crystals. Best performance was achieved with an 11 mm lithium triborate (LBO) crystal at wavelengths of 1046.7 nm and 523.4 nm, respectively. The recorded second-harmonic power is a sum of the two outputs as indicated in the figure. The ratio between these two was nearly unity. In fact the deviation of the two beams can be well placed within a band of 2.5 % as depicted in Fig. 7. The residual fundamental output was only a few milliwatts. The output power could be increased in a cavity configuration with larger footprints 190 mm for the longer arm and 65 mm for the shorter arm. The output characteristics are shown in Fig. 8. Here, a larger volume could be pumped compared to the compact cavity configuration due to a bigger pump spot. The highest extracted output power was 7.2 W with a spectrally clean emission locked to 523.6 nm. The spectral width at a 20 dB clip level was determined as 0.6 nm. We observed a higher output power although for the corresponding fundamental wavelength of 1047.3 nm, there is a larger offset to the target

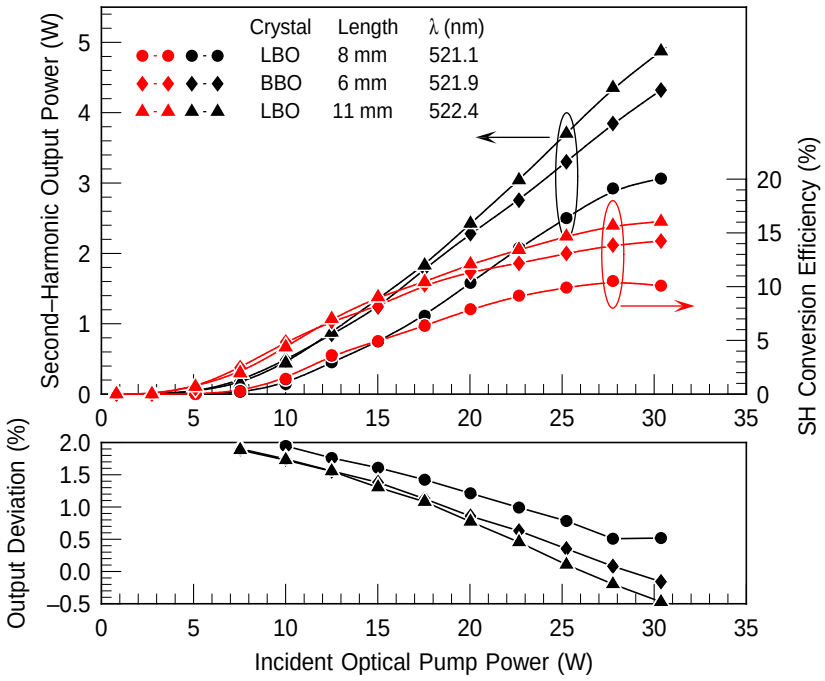

Fig. 7: Top: second-harmonic output characteristics for different materials and lengths of nonlinear crystals in a compact cavity setup. The outputs refer to a locked wavelength provided in the diagram. Bottom: relative power deviation of the two output beams.

wavelegth of 1040 nm. Since the fundamental ouput is higher at longer wavelengths than 1040 nm and the crystals still effectually convert at slightly longer or shorter wavelengths than 520 nm when the angle is changed the frequency conversion was more efficient. The best overall optical-to-optical conversion for this device was roughly 20 %. The maximum

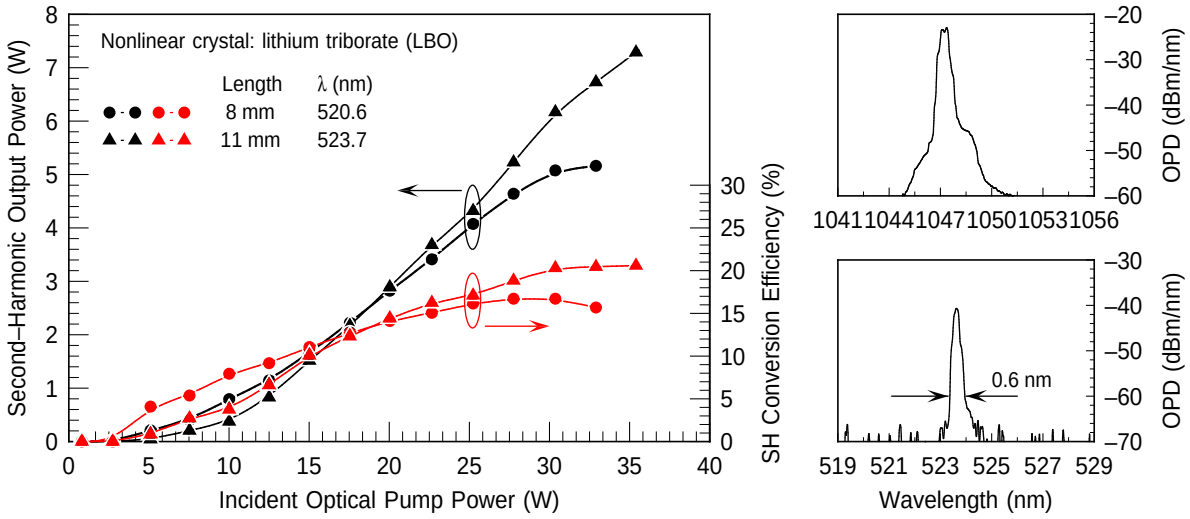

Fig. 8: Second-harmonic output power and optical-to-optical effeciency for different crystal lengths in a larger cavity with the respective wavelengths (left). Optical spectra of the fundamental and second-harmonic regime for the case of an 11 mm long LBO crystal (right).

second-harmonic output and also the conversion efficiency are believed to be limited by the mentioned detuning between the free running wavelength of the laser (1055–1060 nm) and the optimum wavelength for the nonlinear crystals (1040 nm).

6. Conclusion and Outlook

We presented a high-power optically pumped green-emitting VECSEL using intra-cavity second-harmonic generation. Disregarding the insufficient match for the wavelength, a bright multi-watt green laser emission has been demonstrated. With a more precise control of the micro-cavity resonance and subsequently a better match in the emission wavelength, the extraction of output powers of 10 W and more at even better efficiencies seem likely.

References

[1] T. Miyoshi, S. Masui, T. Okada, T. Yanamoto, T. Kozaki, S. Nagahama, and T. Mukai, "510–515 nm InGaN-based green laser diodes on c-plane GaN substrate", *Appl. Phys. Expr.*, vol. 2, pp. 062201-1–3, 2009.

[2] J. Lee, S. Lee, T. Kim, and Y. Park, "7 W high-efficiency continuous-wave green light generation by intracavity frequency doubling of an end-pumped vertical external-cavity surface-emitting semiconductor laser", *Appl. Phys. Lett.*, vol. 89, pp. 241107-1–3, 2006.

[3] J. Chilla, Q. Shu, H. Zhou, E. Weiss, M. Reed, and L. Spinelli, "Recent advances in optically pumped semiconductor lasers", Proc. SPIE 6451, 645109-1–10, 2007

[4] S. Cho, G.B. Kim, J.-Y. Kim, K.-S. Kim, S.-M. Lee, J. Yoo, T. Kim, and Y. Park, "Compact and efficient green VECSEL based on novel optical end-pumping scheme", *IEEE Photon. Technol. Lett.*, vol. 19, pp. 1325–1327, 2007.

[5] R. Hartke, E. Heumann, G. Huber, M. Kühnelt, and U. Steegmüller, "Efficient green generation by intracavity frequency doubling of an optically pumped semiconductor disk laser", *Appl. Phys. B*, vol. 87, pp. 95–99, 2007.

[6] A. Hein, F. Demaria, A. Kern, S. Menzel, F. Rinaldi, R. Rösch, and P. Unger, "Efficient 460-nm second-harmonic generation with optically pumped semiconductor disk lasers", *IEEE Photon. Technol. Lett.*, vol. 23, pp. 179–181, 2011.

[7] S. Beyertt, U. Brauch, F. Demaria, N. Dhidah, A. Giesen, T. Kübler, S. Lorch, F. Rinaldi, and P. Unger, "Efficient gallium-arsenide disk lasers", *IEEE J. Quantum Electron.*, vol. 43, pp. 869–875, 2007.

[8] T. Wang, Y. Kaneda, J.-M. Yarborough, J. Hader, J.V. Moloney, A. Chernikov, S. Chatterjee, S.W. Koch, B. Kunert, and W. Stolz, "High-power optically pumped semiconductor laser at 1040 nm", *IEEE Photon. Technol. Lett.*, vol. 22, pp. 661–663, 2010.